Defect-mediated ferromagnetism in ZnO:Mn nanorods

S. Yılmaz [1,2,3 *], E. McGlynn [1], E. Bacaksız [2], J. Bogan [4]

[1] School of Physical Sciences and National Centre for Plasma Science and Technology, Dublin City University, Glasnevin, Dublin 9, Ireland

[2] Department of Physics, Faculty of Sciences, Karadeniz Technical University, 61080 Trabzon, Turkey

[3] Department of Material Engineering, Faculty of Engineering and Natural Sciences, Adana Science and Technology University, 01180 Adana, Turkey

[4] School of Physical Sciences and National Centre for Sensor Research, Dublin City University, Glasnevin, Dublin 9, Ireland

[*] Corresponding author: Tel: +90 322 455 00 00 fax: +90 322 455 00 09
E-mail: slh_yilmaz@yahoo.com.tr (S. Yılmaz)

Abstract

In this work, the structural, chemical and magnetic properties of ZnO:Mn nanorods were investigated. Firstly, well-aligned ZnO nanorods with their long axis parallel to the crystalline *c*-axis were successfully grown by the vapor phase transport technique on Si substrates coated with a ZnO buffer layer. Mn metal was then diffused into these nanorods at different temperatures in vacuum. From SEM results, ZnO:Mn nanorods were observed to have diameters of ~100 nm and lengths of 4 µm. XPS analysis showed that the Mn dopant substituted into the ZnO matrix with a valence state of +2. Magnetic measurements performed at room temperature revealed that undoped ZnO nanorods exhibit ferromagnetic behavior which may be related to oxygen vacancy defect-mediated d^0 ferromagnetism. ZnO:Mn samples were seen to show an excess room temperature ferromagnetism that is attributed to the presence of oxygen vacancy defects forming bound magnetic polarons involving Mn.

Keywords: ZnO:Mn; Nanorods; XPS; Ferromagnetism

1. Introduction

One-dimensional (1-D) nanomaterials have drawn a lot of interest due to their novel and unique properties and a large number of potential applications such as nanowire field-effect-transistors, nanolasers and nanogenerator [1,2]. ZnO nanomaterials are among the most important one-dimensional (1-D) nanomaterials due to their semiconducting, piezoelectric, and biocompatible properties. ZnO nanomaterials have been found to have a wide range of morphologies such as nanorods, nanotubes, nanobelts and nanorings and the shape and size of such nanostructures play an important role for the performance of the devices [3,4]. There has also been a great deal of attention in ZnO material because of its prospects in optoelectronic applications including chemical sensors, solar cells and optoelectronic devices owing to its direct wide band gap of 3.37 eV at room temperature with a large exciton binding energy (60 meV) [5]. In recent years, ZnO has also become an important material in the search for high Curie temperature (T_c) diluted magnetic semiconductor (DMS) after Dietl's prediction on ZnO:Mn showing ferromagnetism above the room temperature [6]. The presence of room temperature ferromagnetism in V, Cr, Fe, Co, or Ni-doped ZnO systems was also theoretically demonstrated by Sato *et. al* [7]. Among all the transition metal ions-doped ZnO, especially Mn-doped ZnO studies have drawn much attention due to the highest magnetic moment of Mn as well as the occupied first half of Mn d band, which forms a stable polarized state [8]. However, there are some experimental works reported on ZnO:Mn with various morphologies, such as bulk [9], thin films [10] and nanoparticles [11] where the magnetism is very sensitive to preparation conditions such as synthesis method, doping content, sintering temperature and annealing environment. For example, $Zn_{0.99}Mn_{0.01}O$ bulk samples prepared by a standard solid-state reaction method exhibited room-temperature ferromagnetism when sintered at a temperature of 500 °C; however, the samples sintered at a higher temperature of 900 °C displayed a linear response, showing a paramagnetic behavior [12]. Hou *et al.* showed that the magnetization of Mn-doped ZnO thin films decreased with annealing in oxygen atmosphere, whereas annealing in vacuum gave rise to increase the magnetization. They explained their data based on the hypothesis that annealing treatments in vacuum increase the number of defects, leading to an enhancement in ferromagnetism whereas annealing in oxygen leads to almost all defects to disappear, concluding the disappearance of ferromagnetism [13]. According to the study made by Wang *et al.* on ZnO:Mn nanoparticles grown by an ultrasonic assisted sol-gel process, ferromagnetic ordering increases with increases in Mn concentrations up to 2 at.%, while for 5 at.%, ferromagnetism is suppressed and a large paramagnetic effect appears [14]. Some studies have also claimed that

ferromagnetism in Mn-doped ZnO originates from impurities (manganese oxide or precipitation of secondary phases) or the replacement of Zn^{2+} by Mn^{2+} in the ZnO host matrix, while other groups have reported that oxygen vacancies cause ferromagnetic ordering in oxide based DMS [15-17]. Thus there is a wide variance between the data reported for samples grown by different methods and for different nano morphologies. The influence of strain, defects and impurities is very hard to disentangle in many of the reported studies and thus there is a clear need for studies of Mn-doped high quality (crystalline and optical) ZnO materials.

In the literature, there are diverse techniques to produce transition metal-doped ZnO materials. These methods contain pulsed laser deposition [18], rf magnetron sputtering [19], spray pyrolysis [20], sol-gel [21] and vapor phase transport method (VPT) [22]. Within all these methods, VPT method is considerably used due to the simple and low-cost equipment and has been utilized to grow ZnO nanostructures of diverse morphology with excellent crystalline and optical quality [23]. To our knowledge, there are not many studies on ZnO:Mn nanorods grown by VPT method. Therefore, our intention is to obtain 1-D and vertically aligned ZnO-based DMS via this method. In this sense, ZnO nanorods were grown on ZnO buffer layer coated Si substrates by VPT technique and Mn metal was then diffused into these nanorods at three different annealing temperatures in vacuum to achieve DMS with a T_c above the room temperature. In addition, we report a relationship between XPS results and magnetic properties of these samples to clarify the origin of the observed room temperature ferromagnetism in our ZnO:Mn nanorods.

2. Experimental details

Vertically aligned ZnO nanorods were deposited on ZnO buffer layer coated Si substrates by a VPT method where ZnO buffer layer was composed of ZnO seeded Si substrates and subsequent a CBD (chemical bath deposition) ZnO growth. All details of three stages of growth procedure can be found in [22,24].

After the nanorods growth, Mn metal was evaporated on the ZnO nanorods by thermal evaporation (Leybold Univex 350) system with a pressure of ~ 6 x 10^{-6} Torr. The amount of manganese deposited onto ZnO nanorods was monitored by a thickness monitor (Inficon XTM/2) and its thickness was adjusted to ~ 5 nm. After the Mn deposition, the samples were annealed in a quartz tube at temperatures going from 500 °C to 700 °C for 8 h with a step of 100 °C in a vacuum of ~ 10^{-2} Torr. The crystal structure of the samples was carried out using a Bruker AXS D8 diffractometer with CuK_α radiation in the range of $2\theta = 20° – 60°$ with a

step of 0.01°. The surface morphology and composition were performed with a Zeiss EVOLS 15 scanning electron microscope (SEM) attached with energy dispersive x-ray spectroscopy (EDS). For all SEM and EDS measurements, an acceleration voltage of 20 kV was used. The chemical composition and bonding at the surface were characterized by using x-ray photoelectron spectroscopy (XPS) with Al Kα radiation (1486.6eV). The C 1s photoelectron peak at 285.0 eV was used as a reference for the charge-correction of binding energies of core level peaks. Magnetization measurements of the samples (M-H and M-T) were conducted using a Quantum Design Physical Property Measurement System (PPMS) with a vibrating sample magnetometer (VSM) module.

3. Results and discussion

XRD patterns of undoped and ZnO:Mn nanorods annealed at 500 °C, 600 °C, 700 °C for 8 h, respectively, in vacuum are illustrated in Fig. 1(a)-(d). Only diffraction peaks from wurtzite ZnO (002) planes were observed, showing a highly *c*-axis preferred orientation perpendicular to the substrate, which is in good agreement with the SEM results shown later. It was not detected any elemental manganese and its oxides such as MnO, Mn_2O_3, Mn_3O_4 and $ZnMn_2O_4$ in XRD pattern of all the samples, indicating that Mn-doping did not significantly alter the wurtzite ZnO structure. The lattice parameter value of *c* was calculated from the (002) peak of ZnO centered at 34.43° and was found to be 5.21 Å. Within the resolution limit of our XRD system, compared to the undoped sample, there are no detectable peak shifts for the ZnO:Mn samples annealed at 500 °C, 600 °C, 700 °C for 8 h. Furthermore, some diffraction peaks in the pattern can be indexed to the (200), (013), (042) and (240) planes of Zn_2SiO_4, in accordance with JCPDS card no, 24-1469, proposing that reactions between the Si, SiO_2 and ZnO may occur during both the heat treatment of the ZnO seed layer and (more probably) the VPT process conducted at high growth temperature [25].

X-ray rocking curve (XRC) measurements were performed to search for the crystallinity of both undoped and ZnO:Mn nanorods. Fig. 2(a)-(d) show the XRC data measured between 0 and 30° from the ZnO (002) diffraction peaks for the same samples displayed in Fig. 1. It is seen that the full width at half-maximum (FWHM) value of the undoped ZnO sample is 3.36°, implying good alignment of the nanorods perpendicular to the substrate surface. Wang and co-workers obtained a similar FWHM value for their Cu-doped ZnO thin films grown by magnetron sputtering method [26]. On the contrary, the study reported by Yanmei and co-workers showed that undoped ZnO nanorods had a larger FWHM value of 10.4° for hyrothermal synthesized ZnO:Ni samples [27]. Upon Mn evaporation

together with annealing, the intensity of the ZnO (002) peak decreases gradually with the increase of annealing temperature with respect to the undoped ZnO. Additionally, the XRC FWHM values of ZnO nanorods increases gradually and reaches to 6.62° for ZnO:Mn nanorods annealed 700 °C for 8 h, broadly consistent with the changes in XRD peak intensities [28]. These results imply that Mn evaporation and the subsequent annealing process caused a broadening in the (002) peak width most probably due to slight alterations in the underlying ZnO buffer layer planarity which affects the alignment of the VPT–grown nanorods.

The morphological properties of ZnO nanorods grown on ZnO buffer layer coated Si substrates were examined by SEM. Fig. 3(a)-(c) illustrate SEM images of ZnO:Mn nanorods annealed at 600 °C for 8 h. Plane and 45° tilted view images of the ZnO:Mn nanorods were presented in Fig. 3(a) and (b), respectively, which indicated that ZnO:Mn samples grew uniformly over a wide area of ZnO buffer layer coated Si substrate. The inset of Fig. 3(a) showed that ZnO:Mn samples had a hexagonal shape with a diameter of ~ 100 nm. A cross-section image of ZnO:Mn nanorods is given in Fig. 3(c), confirming that ZnO:Mn nanorods were vertically grown on ZnO buffer layer coated Si substrate and all nanorods nearly exhibited similar length of 4.0 µm.

EDS measurements were made to determine the chemical composition of both undoped and ZnO:Mn nanorods. To search for the homogeneity of the samples, elemental mapping was also performed by using EDS. Fig. 4(a) illustrates the SEM image of ZnO:Mn nanorods annealed at 600 °C for 8 h. EDS mapping of Zn, O and Mn elements is presented in Fig. 4(b)-(d), respectively, exhibiting a uniform distribution of the all elements in the sample. Furthermore, it was obtained that the atomic ratio of Mn/Zn+O had a maximum value of ~ 1.7 at.% for ZnO:Mn annealed at 600 °C for 8 h, whereas the atomic ratios of Mn/Zn+O of all the other ZnO:Mn samples exhibited slightly lower values, as listed in Table 1.

Analysis of the valence bonding state of undoped and ZnO:Mn nanorods annealed at 700 °C for 8 h was performed using XPS and is shown in Fig. 5. XPS measurements present evidence for the incorporation of doped ions into the host lattice and the nature of the incorporation. Fig. 5(a) illustrates the full-range XPS survey spectrum and only peaks corresponding to Zn, Mn, O and C are identified. Fig. 5(b) indicates the Mn 2p spectrum for ZnO:Mn nanorods annealed at 700 °C for 8 h. From Fig. 5(b), the core levels of Mn 2p3/2 and 2p1/2 curves were fitted by Gaussian functions and peak values at 641.52 and 653.43 eV were found for Mn 2p3/2 and 2p1/2, respectively, revealing the presence of Mn^{2+} ions in the sample rather than metallic Mn (637.7 eV), Mn^{3+} (642.9 eV) or Mn^{4+} (645.0 eV) [29,30],

which is consistent with other reports [31,32]. These XPS data, combined with the XRD results shown earlier, indicate that the Mn ions substitute on the Zn sites of the ZnO lattice. Fig. 5(c) illustrates the asymmetric O 1s peak of undoped ZnO nanorods, which is deconvoluted into three sub-peaks at the binding energies of 530.68, 531.65 and 532.10 eV. The low binding energy component (labeled as O_L) is ascribed to O^{2-} ions in the wurtzite structure of the hexagonal Zn^{2+} ion array [33], whereas the high binding energy component (denoted as O_H) is related to the presence of loosely bound oxygen on the surface of the ZnO sample belonging to a specific species, such as CO_3, adsorbed H_2O or O_2 [34]. Another peak located at 531.65 eV (marked as O_M) is associated with O^{2-} in oxygen deficient regions within the ZnO matrix, showing the existence of some oxygen vacancies in the sample. The fitted contributions of O_L, O_M and O_H peaks are presented in Fig. 5(c)-(d) and the areas of these fitted peaks are denoted by A_L, A_M and A_H, respectively. For undoped ZnO nanorods shown in Fig. 5(c), the ratio of $A_M/A_L+A_M+A_H$ is determined to be ~ 0.21. However, in Fig. 5(d), this ratio increased to ~ 0.36 for ZnO:Mn nanorods annealed at 700 °C for 8 h, which is a clear indication of the growth of a significant population of V_o defects induced by Mn-doping. A similar analysis for ZnO thin films was also carried out by Can *et al.* [35].

Magnetization loops of all ZnO nanorods were measured at 300 K using a VSM. The effect of Si substrate was eliminated to have an actual magnetization of the samples. The M-H loop of a bare Si substrate is shown in the inset at the upper left side of Fig. 6, approving that Si has pure diamagnetic behavior. Fig. 6(a)-(d) shows the room temperature M-H curves of undoped and ZnO:Mn nanorods annealed at 500 °C, 600 °C, 700 °C for 8 h in vacuum, respectively. It can be seen that both undoped and ZnO:Mn samples are ferromagnetic in nature. Ghosh *et al.* found a similar ferromagnetic behavior for nominally undoped ZnO in their K-doped ZnO nanowires [36]. The reason for the observed ferromagnetism in nominally undoped ZnO nanorods is probably due to the oxygen vacancy defect-induced d^0 ferromagnetism [37,38]. The nominally undoped ZnO nanorods have a saturation magnetization (M_s), remnant magnetization (M_r) and coercive field (H_c) values of 0.13 emu/gr, 0.02 emu/gr and 210 Oe, respectively. Data from an (otherwise identical) nominally undoped ZnO sample annealed at 700 °C for 8 h in vacuum is also presented in Fig. 6(e) where the annealed nominally undoped ZnO nanorods have M_s, M_r and H_c values of 0.13 emu/gr, 0.03 emu/gr and 197 Oe, respectively, indicating that annealing in vacuum alone does not markedly change the M_s value of the nanorods with respect to unannealed nominally undoped ZnO. However, after annealing the ZnO:Mn nanorods at 500 °C and 600 °C in vacuum, it was seen that M_s values increased to 0.16 emu/gr and 0.18 emu/gr, respectively.

With a further increase in annealing temperature to 700 °C, a maximum M_s value of 0.19 emu/gr was obtained for ZnO:Mn samples, confirming the definite role of Mn-doping in enhancing the ferromagnetism. As compared to unannealed nominally undoped ZnO, the ZnO:Mn samples annealed at 500 °C, 600 °C and 700 °C for 8 h have larger M_s values, and specifically the ZnO:Mn sample annealed at 700 °C for 8 h has a larger M_s value than that of the annealed nominally undoped sample. In all the annealed samples, based on the discussion above there is an appreciable concentration of intrinsic defects. The existence of a high population of intrinsic defects like oxygen vacancy (V_o) in the structure, in addition to the Mn-doping, causes an increase in the number of bound magnetic polarons (BMPs). According to the BMP theory, magnetic cations (Mn^{2+}), electronic carriers and intrinsic/native defects can form BMPs. An electron associated with a native defect such as an oxygen vacancy will be confined in a hydrogenic orbit of radius r_H to form a hydrogen atomic-like structure. BMPs can be formed by the exchange interaction between such electrons and magnetic cations (Mn^{2+}) residing within the orbit radius (r_H) of electrons. Ferromagnetism results when the BMPs begin to overlap to form a continuous chain throughout the material. Therefore, a greater density of native defects in conjunction with Mn doping helps to produce more BMPs which yields a greater overall volume occupied by BMPs, leading to the overlap of BMPs, resulting in an ferromagnetism [39]. Liu *et al*. grew Mn-doped ZnO nanowires via chemical vapor deposition at substrate temperatures of 750 °C, 850 °C and 950 °C. Paramagnetic behavior was observed for the samples grown at 750 °C and 850 °C due to a formation of $ZnMn_2O_4$, whereas they found that ZnO:Mn nanowires synthesized at 950 °C exhibited room temperature ferromagnetism, attributed to a greater substitution of Mn^{2+} into the ZnO matrix, leading to ferromagnetic ordering with a M_s of 0.25 emu/gr [40]. In our study, compared with nominally undoped (annealed and unannealed) and all the other ZnO:Mn nanorods, ZnO:Mn annealed at 700 °C for 8 h has the lowest M_r values of 0.01 emu/gr and H_c of 36 Oe which is indicative of a small hysteresis area, meaning that the sample displays soft ferromagnet behavior [16]. We note that in general the observed room temperature ferromagnetism in ZnO:Mn nanorods could also possibly arise from other sources such as inclusions of impurity clusters/phases. In this regard, Mn, MnO, MnO_2 and Mn_2O_3 phases are well-known to be antiferromagnetic with Neel temperatures of 100, 116, 92 and 76 K, respectively, whereas Mn_3O_4 is ferromagnetic with a Curie temperature of 43 K [13,41]. However, the origin of ferromagnetism in our samples is not due to the existence of manganese oxides and clusters because these secondary phases were not observed in the ZnO:Mn nanorods either by XRD or by XPS measurements.

Among all the ZnO:Mn nanorod samples, the maximum M_s value of 0.19 emu/gr was obtained for Mn diffusion-doped ZnO annealed at 700 °C for 8 h, corresponding to the 0.27 μ_B/Mn. However, this value is significantly smaller than theoretical value (5.92 μ_B/Mn) for a free Mn^{2+} ion with S = 5/2 and g = 2, suggesting either (i) that not all the Mn ions are effectively involved in BMP formation or (ii) the presence of a competition between the antiferromagnetic and ferromagnetic interactions of closely spaced Mn ions. Due to the strong antiferromagnetic interactions between neighboring Mn ions, ferromagnetic ordering can be suppressed. Both these effects may contribute to the observation that the magnetization of Mn ions that is much lower than that based on a simple theoretical estimate [42].

We note finally that in the literature some other possible models have been suggested to explain the origin of dopant-related ferromagnetism in transition metal (TM)-doped ZnO including the double exchange mechanism proposed by Garcia *et al.*, based on the co-existence of Mn^{3+} and Mn^{4+} oxidation states in ZnO:Mn [43] and the RKKY (Ruderman-Kittel-Kasuya-Yosida) model where the magnetism results from the exchange interaction between local spin-polarized electrons (such as electrons of Mn^{2+} ions) and conduction electrons, with the concentration of free carriers playing a crucial role in establishing the ferromagnetism. The double-exchange mechanism did not apply for our case due to the presence of Mn^{2+} in our ZnO:Mn nanorods. The RKKY mechanism also does not seem to be relevant in explaining the ferromagnetism in our Mn-doped samples due to the expected resistive nature of ZnO:Mn samples compared to undoped ZnO. Reports in the literature for ZnO samples grown by the VPT method (similar to our samples) reveal a carrier concentration in the order of 10^{17} cm^{-3} [44] and doping with Mn led to a decrease in the carrier concentration and an increase in the resistivity. For example, Hong et al. synthesized Mn-doped ZnO thin films by PLD and observed that Mn-doping decreased the carrier concentration and increased the resistivity of ZnO films [45]. In addition, Lin et al. produced Mn-doped ZnO thin films by plasma-assisted molecular beam epitaxy and found that the carrier concentration of undoped ZnO ($3.23x10^{18}cm^{-3}$) decreased with an increase of Mn-doping to 9.5 % ($2.14x10^{15}$ cm^{-3}) [46].

Based on the entirety of the discussion above we believe that the observed excess room temperature ferromagnetism in the ZnO:Mn samples (compared to annealed nominally undoped samples) is due to Mn-related BMP formation, as explained above. The BMP model is consistent with our XPS results and leads us to conclude that our ZnO:Mn nanorods include a large amount of intrinsic defects (like V_o) induced by the Mn-doping, which give rise to

favourable conditions for the formation of Mn-related BMPs, and hence to room temperature ferromagnetism.

In order to determine the Curie temperature (T_c), the magnetization versus temperature (M-T) was done in the temperature range of 5-300 K at an applied magnetic field of 500 Oe for ZnO:Mn nanorods annealed at 700 °C for 8 h, and the data are indicated in Fig. 7. From these data, it can be seen that the magnetization was significantly reduced with an increase of the temperature up to 300 K. It is well-known that the Curie temperature corresponds to the point where the magnetization drops to zero and the material goes from magnetically ordered to disordered. In light of this, it can be said that the Curie temperature for our sample is above the room temperature, however it is not possible to determine the exact value because it goes beyond the range of our experimental capabilities. Some studies showed that Mn-doped ZnO indicates ferromagnetism with Curie temperatures above room temperature and our result is consistent with these reports [13,47].

4. Conclusions

In summary, the following points can be concluded from our studies: (i) XRD and SEM results showed that all the samples had wurtzite structure with a well-aligned nanorod morphology; (ii) the XPS results indicated that Mn ions successfully substituted for Zn ions in the lattice and ZnO:Mn nanorods also had a large concentration of native defects (oxygen vacancies) compared to undoped ZnO; (iii) magnetic measurements illustrated that undoped and ZnO:Mn samples showed the room temperature ferromagnetism; (iv) comparing magnetic data with the XPS data, it is concluded that the observed excess ferromagnetism in ZnO:Mn nanorods can be related to the formation of Mn-related BMP, associated with an exchange interaction between Mn^{2+} ions and oxygen vacancy defect-bound carriers.

Acknowledgments

SY is grateful to the Council of Turkish Higher Education for its financial support to visit foreign institutions. This work was supported by the research fund of Karadeniz Technical University, Trabzon, Turkey, under contract no. 2010.111.001.3. EMcG gratefully acknowledges support from the Science Foundation Ireland Strategic Research Cluster grant entitled “Functional Oxides and Related Materials for Electronics” (FORME). All the authors also would like to thank Prof. Dr. Ş. Özcan and Assoc. Prof. Dr. A. Ceylan for their efforts on magnetic measurements. All XPS analysis of the work were performed by Dr. M. Çopuroğlu in the Department of Chemistry of Bilkent University in the leadership of Prof. Dr. Ş. Süzer.

References

[1] M.H. Huang, S. Mao, H. Feick, H. Yan, Y. Wu, H. Kind, E. Weber, R. Russo, P. Yang, Science **292**, 1897 (2001)

[2] X. Wang, J. Song, J. Liu, Z.L. Wang, Science **316,** 102 (2007)

[3] D. Pradhan, Z. Su, S. Sindhwani, J.F. Honek, K.T. Leung, J. Phys. Chem. C **115,** 18149 (2011)

[4] M. Biswas, E. McGlynn, M.O. Henry, M. McCann, A. Rafferty, J. Appl. Phys. **105,** 094306 (2009)

[5] P.D. Batista, M. Mulato, Appl. Phys. Lett. **87,** 143508 (2005)

[6] T. Dietl, H. Ohno, F. Matsukura, J. Cibert, D. Ferrand, Science **287,** 1019 (2000)

[7] K. Sato, H. Katayama-Yoshida, Jpn. J. Appl. Phys. Part 2 **39,** L555 (2000)

[8] P. Sharma, A. Gupta, K.V. Rao, F.J. Owens, R. Sharma, R. Ahuja, J.M.O. Guillen, B. Johansson, G.A. Gehring, Nat. Mater. **2,** 673 (2003)

[9] S-J. Han, T.-H. Jang, Y.B. Kim, B.-G. Park, J.-H. Park, Y.H. Jeong, Appl. Phys. Lett. **83,** 920 (2003)

[10] J. Elanchezhiyan, K.P. Bhuvana, N. Gopalakrishnan, T. Balasubramanian, J. Alloys Compd. **463,** 84 (2008)

[11] C.J. Cong, L. Liao, J.C. Li, L.X. Fan, K.L. Zhang, Nanotechnology **16,** 981 (2005)

[12] J. Zhang, R. Skomski, D.J. Sellmyer, J. Appl. Phys. **97,** 10D303 (2005)

[13] D.L. Hou, X.J. Ye, H.J. Meng, H.J. Zhou, X.L. Li, C.M. Zhen, G.D. Tang, Mater. Sci. Eng. B **138,** 184 (2007)

[14] J.B. Wang, G.J. Huang, X.L. Zhong, L.Z. Sun, Y.C. Zhou, E.H. Liu, Appl. Phys. Lett. **88,** 252502 (2006)

[15] H.B. Wang, H. Wang, C. Zhang, F.J. Yang, C.P. Yang, H.S. Gu, M.J. Zhou, Q. Li, Y. Jiang, Mater. Chem. Phys. **113,** 884 (2009).

[16] O.D. Jayakumar, H.G. Salunke, R.M. Kadam, M. Mohapatra, G. Yaswant, S.K. Kulshreshtha, Nanotechnology **17,** 1278 (2006)

[17] H.L. Yan, X.L. Zhong, J.B. Wang, G.J. Huang, S.L. Ding, G.C. Zhou, Y.C. Zhou, Appl. Phys. Lett. **90,** 082503 (2007)

[18] X.L. Wang, K.H. Lai, A. Ruotolo, J. Alloys Compd. **542,** 147 (2012)

[19] C.G. Jin, T. Yu, Z.F. Wu, X.M. Chen, X.M. Wu, L.J. Zhuge, Appl. Phys. A **109,** 173 (2012)

[20] S. Yılmaz, M. Parlak, Ş. Özcan, M. Altunbaş, E. McGlynn, E. Bacaksız, Appl. Surf. Sci. **257,** 9293 (2011)

[21] P. Varshney, G. Srinet, R. Kumar, V. Sajal, S.K. Sharma, M. Knobel, J. Chandra, G. Gupta, P.K. Kulriya, Mater. Sci. Semicond. Process. **15,** 314 (2012)
[22] S. Yılmaz, E. McGlynn, E. Bacaksız, Ş. Özcan, D. Byrne, M.O. Henry, R.K. Chellappan, J. Appl. Phys. **111,** 013903 (2012)
[23] R.T.R. Kumar, E. McGlynn, M. Biswas, R. Saunders, G. Trolliard, B. Soulestin, J.-R. Duclere, J.P. Mosnier, M.O. Henry, J. Appl. Phys. **104,** 084309 (2008)
[24] D. Byrne, E. McGlynn, K. Kumar, M. Biswas, M.O. Henry, G. Hughes, Cryst. Growth Des. **10,** 2400 (2010)
[25] D. Byrne, R.F. Allah, T. Ben, D.G. Robledo, B. Twamley, M.O. Henry, E. McGlynn, Cryst. Growth Des. **11,** 5378 (2011)
[26] X.B. Wang, C. Song, K.W. Geng, F. Zeng, F. Pan, Appl. Surf. Sci. **253,** 6905 (2007)
[27] L. Yanmei, W. Tao, S. Xia, F. Qingqing, L. Qingrong, S. Xueping, S. Zaoqi, Appl. Surf. Sci. **257,** 6540 (2011)
[28] E. McCarthy, R.T.R. Kumar, B. Doggett, S. Chakrabarti, R.J. O'Haire, S.B. Newcomb, J.-P. Mosnier, M.O. Henry, E. McGlynn, J. Phys. D: Appl. Phys. **44,** 375401 (2011)
[29] R.K. Singhal, M.S. Dhawan, S.K. Gaur, S.N. Dolia, S. Kumar, T. Shripathi, U.P. Deshpande, Y.T Xing,. E. Saitovitch, K.B. Garg, J. Alloys Compd. **477,** 379 (2009)
[30] X. Yan, D. Hu, H. Li, L. Li, X. Chong, Y. Wang, Physica B **406,** 3956 (2011).
[31] W.B. Mi, H.L. Bai, H. Liu, C.Q. Sun, J. Appl. Phys. **101,** 023904 (2007)
[32] D. Wang, S. Park, Y. Lee, T. Eom, S. Lee, Y. Lee, C. Choi, J. Li, C. Liu, Cryst. Growth Des. **9,** 2124 (2009)
[33] U. Ilyas, R.S. Rawat, T. L. Tan, P. Lee, R. Chen, H. D. Sun, L. Fengji, S. Zhang, J. Appl. Phys. **111,** 033503 (2012)
[34] U. Ilyas, R.S. Rawata, G. Roshana, T.L. Tana, P. Leea, S.V. Springhama, S. Zhangc, L. Fengjic, R. Chend, H.D. Sund, Appl. Surf. Sci. **258,** 890 (2011)
[35] M.M. Can, S.I. Shah, M.F. Doty, C.R. Haughn, T. Fırat, J. Phys. D: Appl. Phys. **45,** 195104 (2012)
[36] S. Ghosh, G.G. Khan, B. Das, K. Mandal, J. Appl. Phys. **109,** 123927 (2011)
[37] G. Xing, D. Wang, J. Yi, L. Yang, M. Gao, M. He, J. Yang, J. Ding, T.C. Sum, T. Wu, Appl. Phys. Lett. **96,** 112511 (2010)
[38] D. Gao, J. Zhang, G. Yang, J. Zhang, Z. Shi, J. Qi, Z. Zhang, D. Xue, J. Phys. Chem. C **114,** 13477 (2010)
[39] J.M.D. Coey, M. Venkatesan, C.B. Fitzgerald, Nat. Mater. **4,** 173 (2005)
[40] J.J. Liu, K. Wang, M.H. Yu, W.L. Zhou, J. Appl. Phys. **102,** 024301 (2007)

[41] C.J. Cong, L. Liao, Q.Y. Liu, J.C. Li, K.L. Zhang, Nanotechnology **17,** 1520 (2006)
[42] J. Zhang, X.Z. Li, J. Shi, Y.F. Lu, D.J. Sellmyer, J. Phys.: Condens. Matter **19,** 036210 (2007)
[43] M.A. Garcia, M.L. Ruiz-Gonzalez, A. Quesada, J.L. Costa-Kramer, J.F. Fernandez, S.J. Khatib, A.Wennberg, A.C. Caballero, M.S. Martin-Gonzalez, M. Villegas, F. Briones, J.M. Gonzalez-Calbet, A. Hernando, Phys. Rev. Lett. **94,** 217206 (2005)
[44] J. Goldberger, D.J. Sirbuly, M. Law, P. Yang, J. Phys. Chem. B **109,** 9 (2005)
[45] N.H. Hong, E. Chikoidze, Y. Dumont, Physica B **404,** 3978 (2009)
[46] H.-J. Lin, D.-Y. Lin, J.-Z. Hong, C.-S. Yang, C.-M. Lin, C.-F. Lin, Phys. Status Solidi C **6,** 1468 (2009)
[47] V.K. Sharma, R. Xalxo, G.D. Varma, Cryst. Res. Technol. **42,** 34 (2007)

Figure Captions

Fig. 1. XRD patterns of nominally undoped ZnO (a) and ZnO:Mn nanorods annealed at 500 °C (b), 600 °C (c), 700 °C (d) for 8 h.

Fig. 2. Rocking curves (of the (002) peak) of nominally undoped ZnO (a) and ZnO:Mn nanorods annealed at 500 °C (b), 600 °C (c), 700 °C (d) for 8 h..

Fig. 3. SEM images of (a) Top view, (b) 45° tilted view obtained from edge of sample and (c) cross-section of ZnO:Mn nanorods annealed at 600 °C for 8 h.

Fig. 4. (a) A SEM image and EDS mapping of (b) Zn, (c) O, (d) Mn elements of ZnO:Mn nanorods sample annealed at 600 °C for 8 h.

Fig. 5. (a) XPS survey spectra of nominally undoped and ZnO:Mn nanorod arrays annealed at 700 °C for 8 h, (b) shows binding energy spectrum of Mn 2p and Gaussian fitting, (c) and (d) illustrate the binding energy spectra of O 1s with Gaussian fitting for undoped ZnO and ZnO:Mn nanorods annealed at 700 °C for 8 h, respectively.

Fig. 6. Room temperature M-H curves of nominally undoped ZnO (a), ZnO:Mn nanorods annealed at 500 °C (b), 600 °C (c), 700 °C (d) for 8 h, and nominally undoped ZnO nanorods annealed at 700 °C for 8 h (e). Inset shows the M-H loop of a bare Si substrate.

Fig. 7. Temperature dependence of magnetization of ZnO:Mn nanorods annealed at 700 °C for 8 h.

Table Captions

Table 1. Actual atomic concentrations of Zn, O or Mn in nominally undoped ZnO and ZnO:Mn nanorods.

Table 1

Sample	Measured at.%		
	Mn	Zn	O
ZnO	-	39.73	60.27
ZnO:Mn annealed at 500 °C for 8 h	1.36	38.44	60.20
ZnO:Mn annealed at 600 °C for 8 h	1.67	40.84	57.49
ZnO:Mn annealed at 700 °C for 8 h	1.02	39.57	59.41

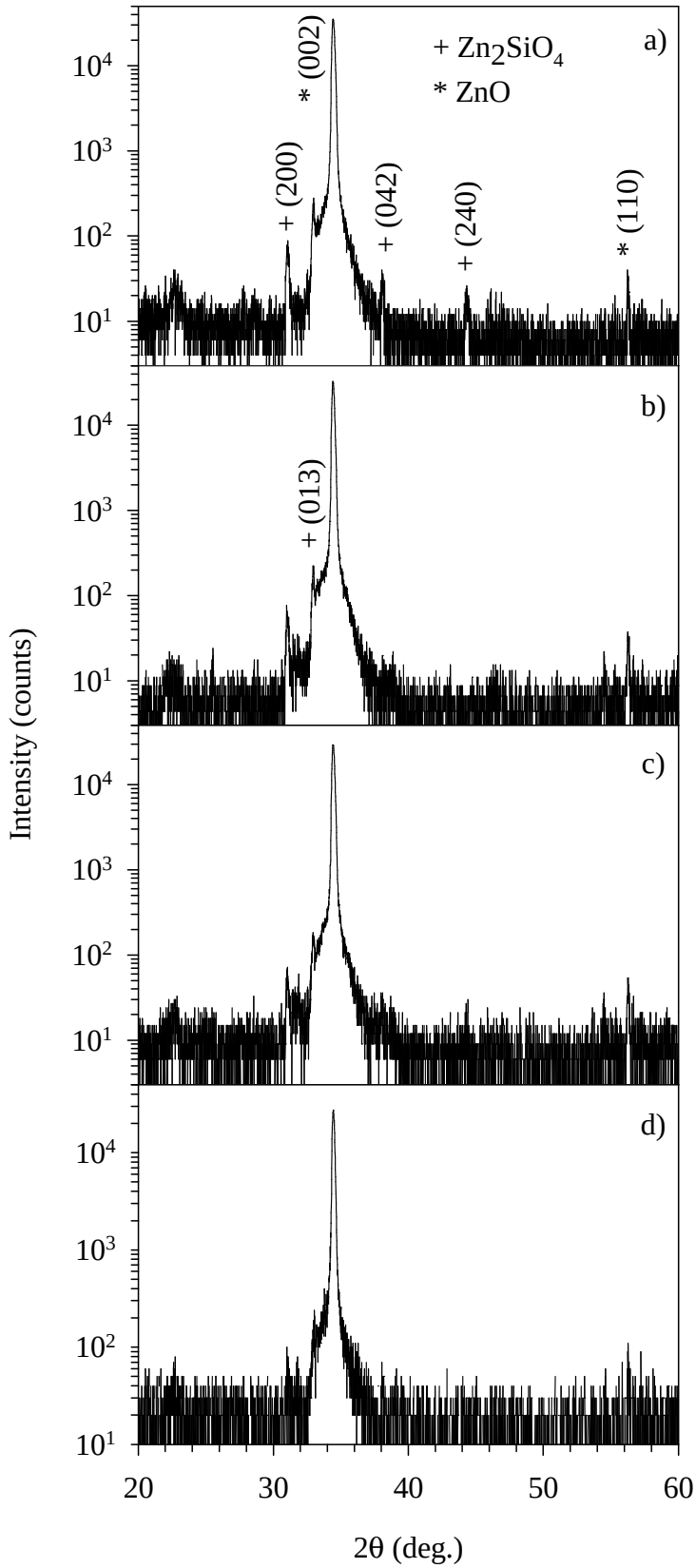
+ Zn_2SiO_4
* ZnO
a)
b)
c)
d)
+ (200)
* (002)
+ (042)
+ (240)
* (110)
+ (013)
Intensity (counts)
2θ (deg.)
10^1
10^2
10^3
10^4
20
30
40
50
60

Fig. 1

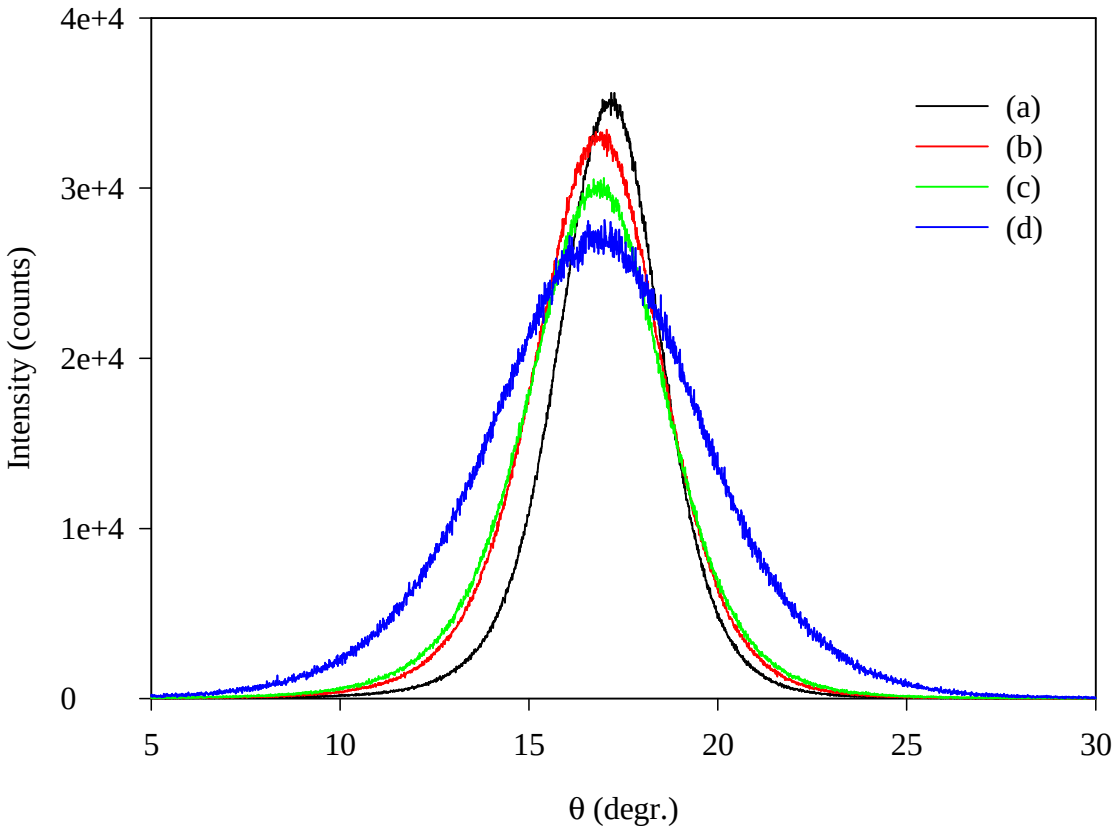

Fig. 2

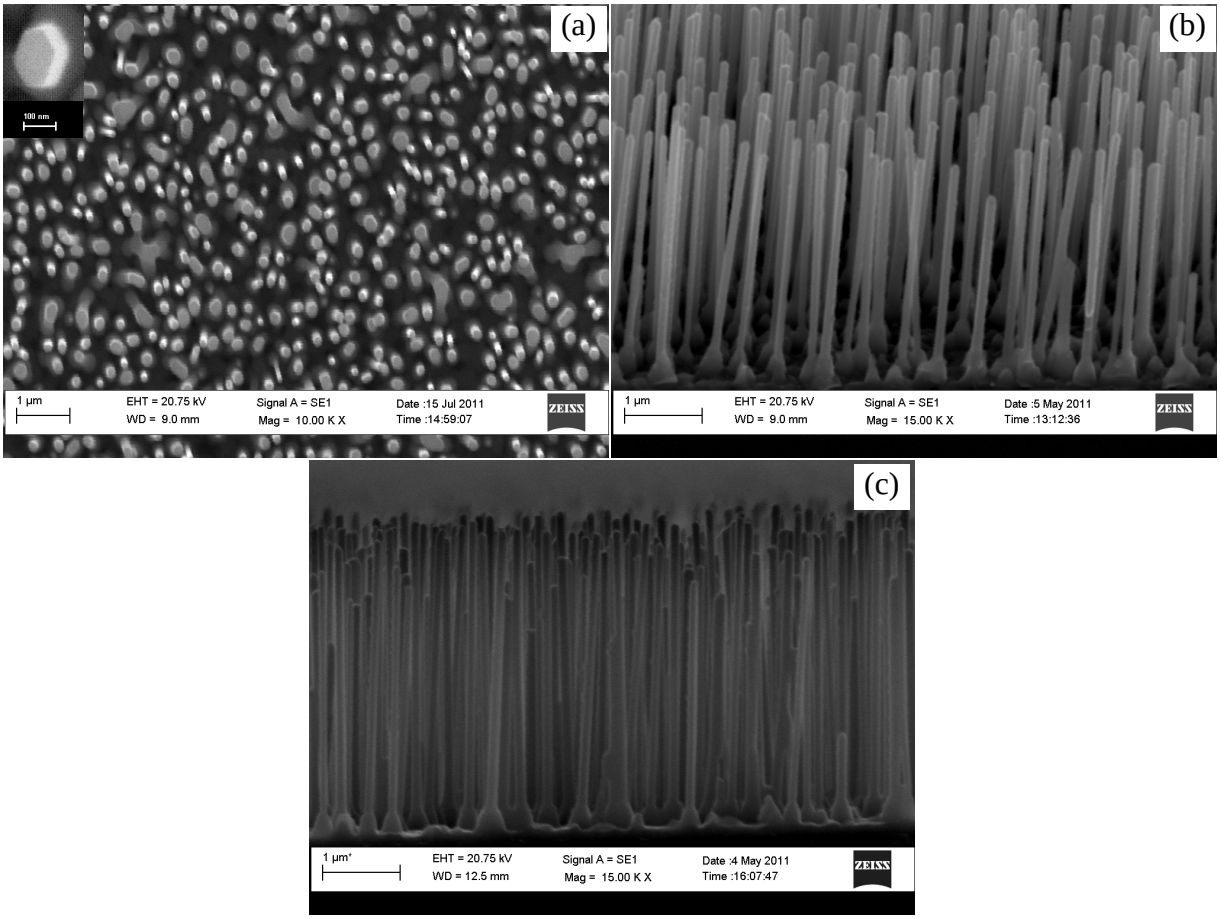
(a)
100 nm
1 µm
EHT = 20.75 kV
WD = 9.0 mm
Signal A = SE1
Mag = 10.00 K X
Date :15 Jul 2011
Time :14:59:07
ZEISS
(b)
1 µm
EHT = 20.75 kV
WD = 9.0 mm
Signal A = SE1
Mag = 15.00 K X
Date :5 May 2011
Time :13:12:36
ZEISS
(c)
1 µm
EHT = 20.75 kV
WD = 12.5 mm
Signal A = SE1
Mag = 15.00 K X
Date :4 May 2011
Time :16:07:47
ZEISS

Fig. 3

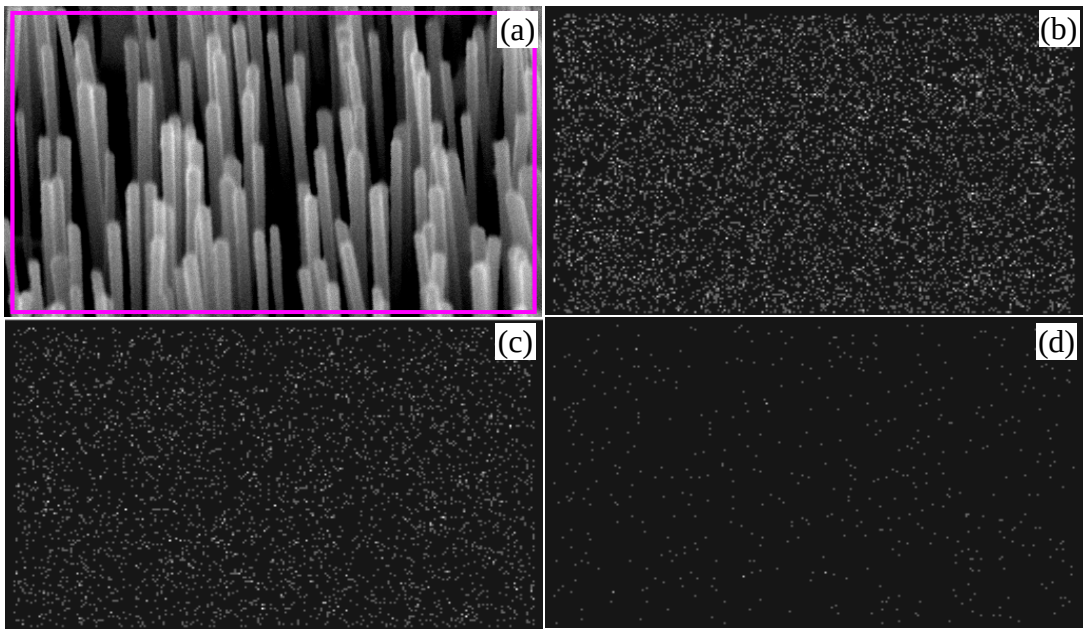

Fig. 4

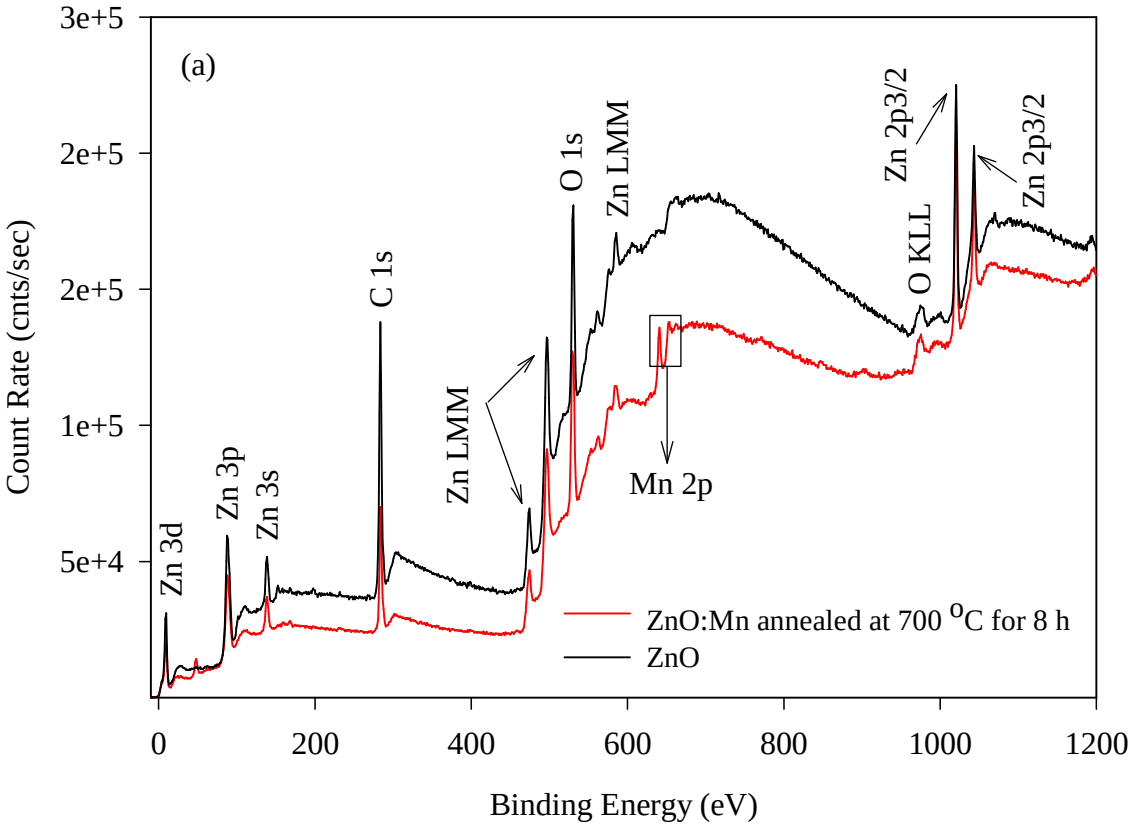
(a)
Count Rate (cnts/sec)
3e+5
2e+5
2e+5
1e+5
5e+4
0
200
400
600
800
1000
1200
Binding Energy (eV)
Zn 3d
Zn 3p
Zn 3s
C 1s
Zn LMM
O 1s
Zn LMM
Mn 2p
O KLL
Zn 2p3/2
Zn 2p3/2
ZnO:Mn annealed at 700 °C for 8 h
ZnO

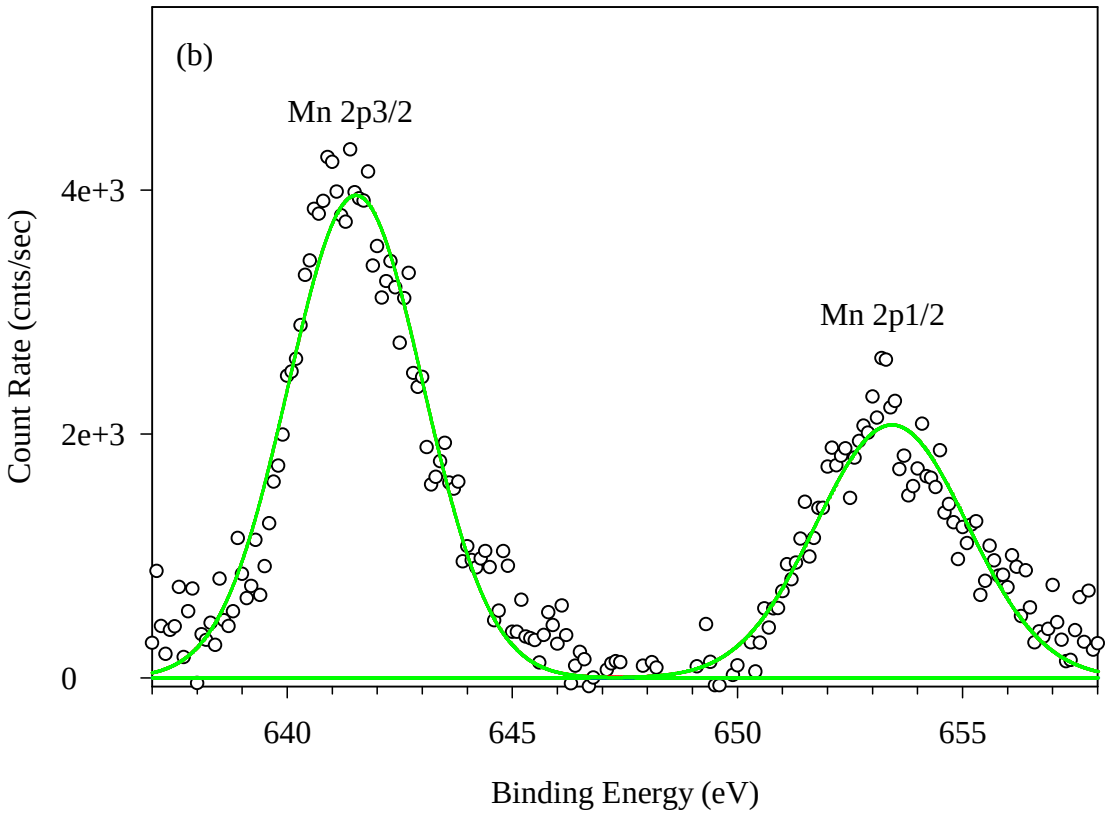
(b)
Mn 2p3/2
Mn 2p1/2
Count Rate (cnts/sec)
4e+3
2e+3
0
640
645
650
655
Binding Energy (eV)

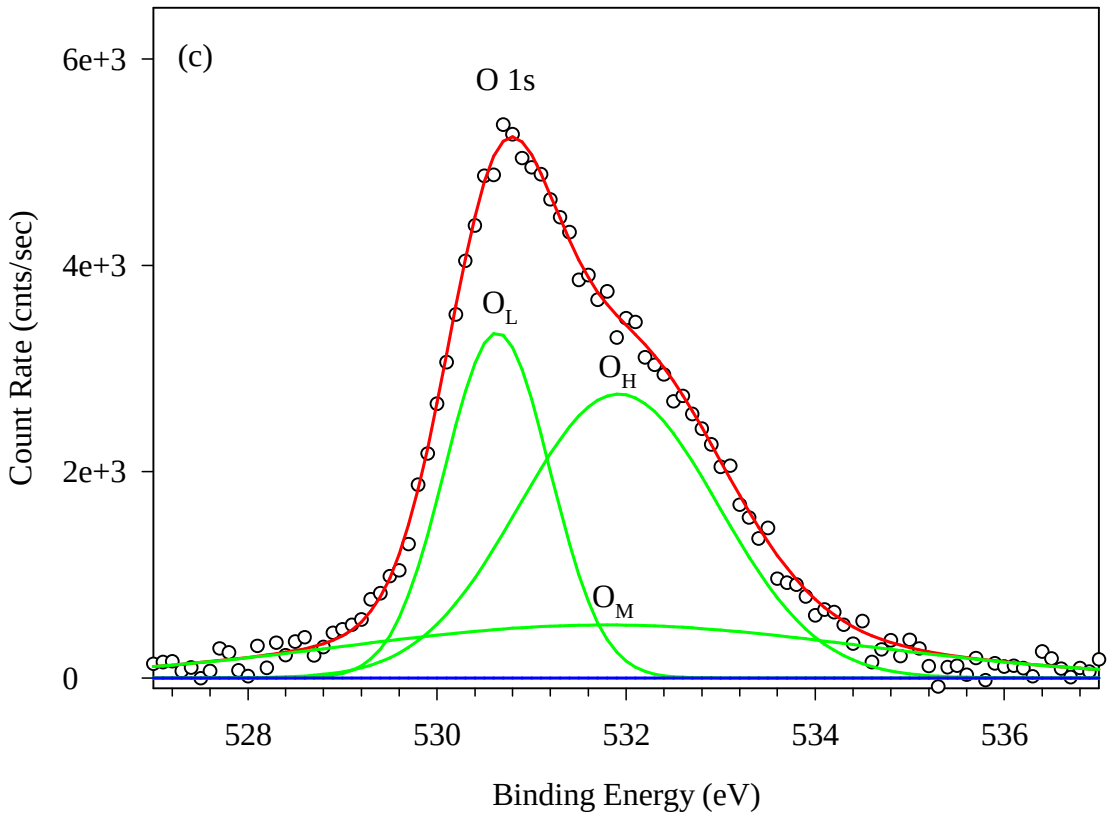
(c)
O 1s
6e+3
4e+3
2e+3
0
Count Rate (cnts/sec)
O_L
O_H
O_M
528
530
532
534
536
Binding Energy (eV)

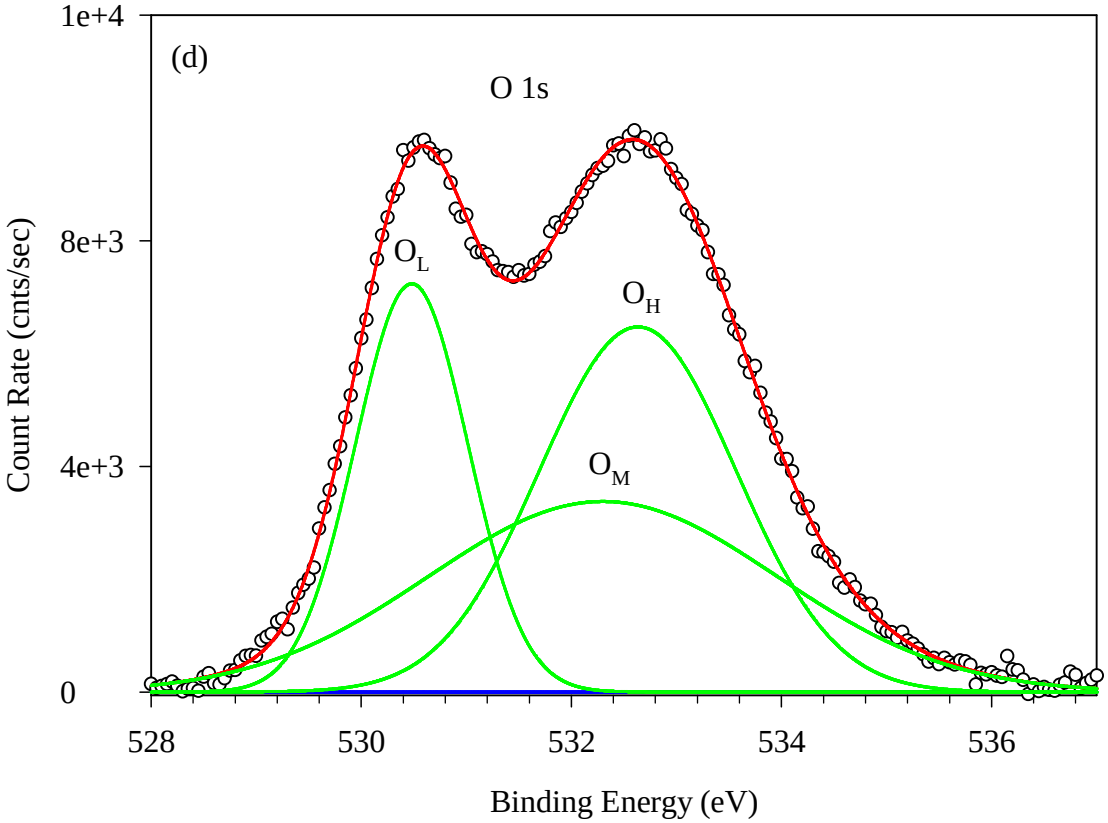
(d)
O 1s
1e+4
8e+3
4e+3
0
Count Rate (cnts/sec)
O_L
O_H
O_M
528
530
532
534
536
Binding Energy (eV)

Fig. 5

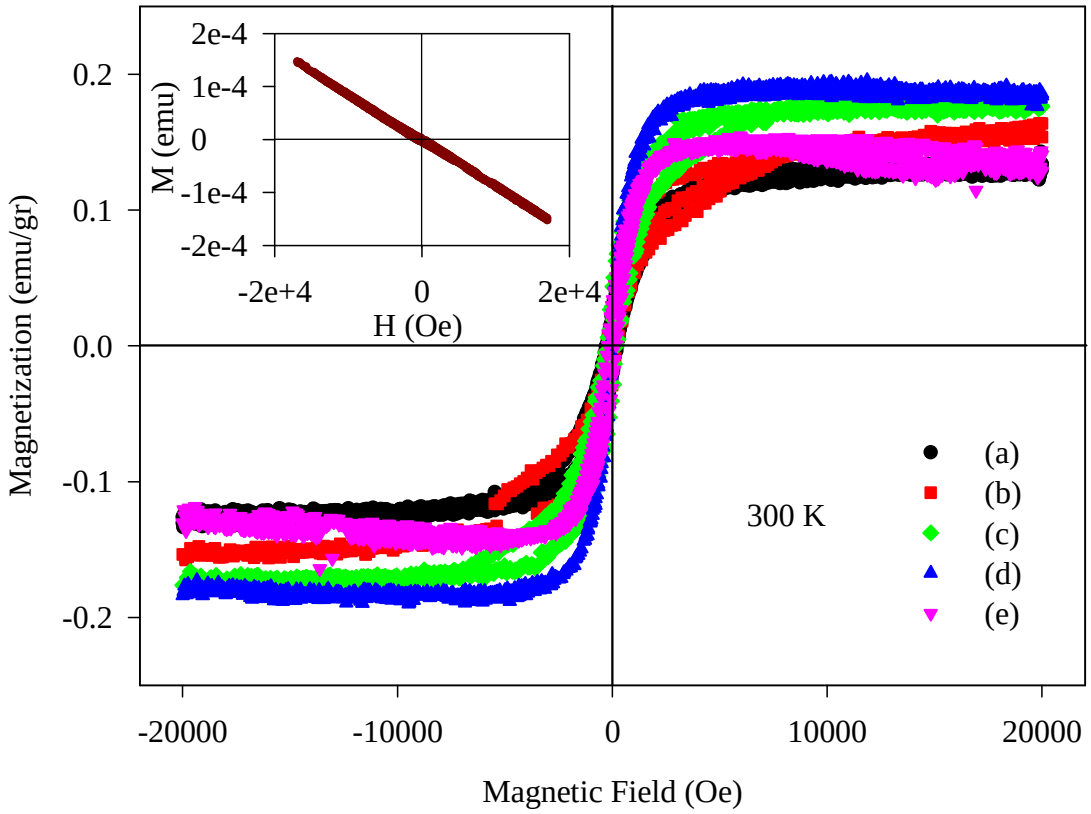
Magnetization (emu/gr)
0.2
0.1
0.0
-0.1
-0.2
-20000
-10000
0
10000
20000
Magnetic Field (Oe)
M (emu)
2e-4
1e-4
0
-1e-4
-2e-4
-2e+4
0
2e+4
H (Oe)
300 K
(a)
(b)
(c)
(d)
(e)

Fig. 6

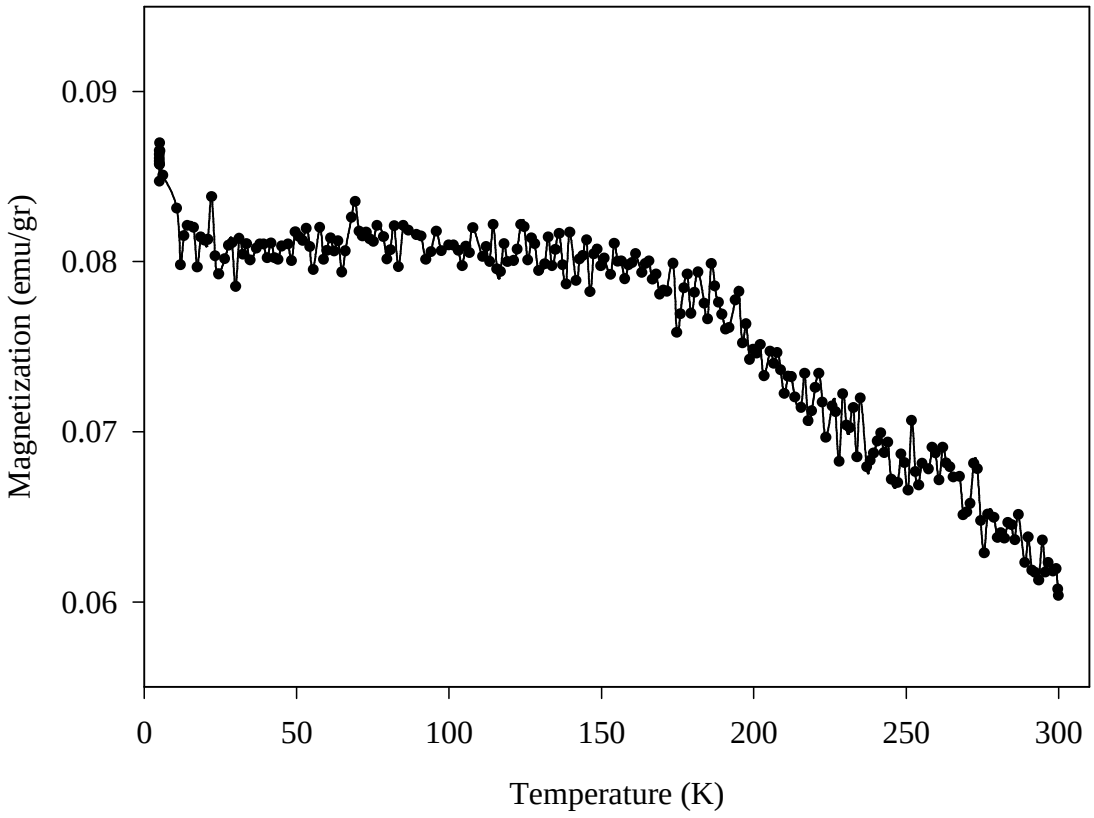
0.09
0.08
0.07
0.06
Magnetization (emu/gr)
0
50
100
150
200
250
300
Temperature (K)

Fig. 7